Journal of Drug Delivery Science and Technology 78 (2022) 103935

Contents lists available at ScienceDirect

Journal of Drug Delivery Science and Technology

journal homepage: www.elsevier.com/locate/jddst

# An ultrasound-enhanced electrospinning for generating multilayered nanofibrous structures

Arle Kõrkjas [a], Kaarel Laar [a], Ari Salmi [b], Joni Mäkinen [b], Edward Hæggström [b], Karin Kogermann [a], Jyrki Heinämäki [a], Ivo Laidmäe [a,c,*]

[a] Institute of Pharmacy, University of Tartu, Tartu, Estonia
[b] Electronics Research Laboratory, Department of Physics, University of Helsinki, Helsinki, Finland
[c] Department of Immunology, Institute of Biomedicine and Translational Medicine, University of Tartu, Tartu, Estonia

ARTICLE INFO

*Keywords:*
ultrasound-Enhanced electrospinning
Multilayered nanofibers
Polyethylene oxide
Nanofiber thickness
Wound healing
Tissue engineering

ABSTRACT

The ability to modify nanofiber diameter on the fly can give an opportunity to create advanced nanofiber materials with complex design. Such flexibility provides possibilities to produce materials with gradient structures (physical and mechanical), desirable in wound healing and tissue engineering applications. We investigated a needleless ultrasound-enhanced electrospinning technique (USES) for generating multilayered nanofiber mats. The aim was to gain understanding of how the process parameters of USES affect the thickness and morphology of nanofibers. Levels of three process parameters were changed in a stepwise manner, permitting us to create multiple layers of nanofibers with different thickness. In the first test we found that by increasing the ultrasound burst rate from 150 Hz to 1800 Hz, the average nanofiber diameter increased by 90 nm. The second test showed a 170 nm decrease in average fiber diameter when ultrasound burst count was increased from 1200 Hz to 10000 Hz. The third set of experiments showed a minimal increase in fiber diameter when the duty cycle was decreased from 11.5% to 1.8%. Fourier transform infrared spectroscopy revealed no process induced transformations when generating nanofibers from aqueous PEO solutions with the USES device. In conclusion, USES enables us to modify nanofiber thickness in real time, and consequently, to generate multiple fiber layers having different average fiber diameter. Therefore, we believe that USES as a novel needleless electrospinning method holds promise for manufacturing of multilayered (gradient) nanofiber structures for wound healing and tissue engineering applications.

## 1. Introduction

Chronic wounds associated with many common chronic disease states are still a major challenge for the health care system, and there are many reasons, why a wound becomes chronic [1]. The most common chronic wounds include diabetic wounds, pressure ulcers, and venous ulcers which make up 70% of chronic wound cases [2]. Chronic "hard-to-heal" wounds often get infected, thus further prolonging and impairing a healing process [3]. There are many factors that need to be considered for successful chronic wound treatment and the availability of proper wound dressings is one part of that. Despite recent advancements, the current standard of wound dressings is unsatisfactory and not very applicable for treating chronic wounds. There's a lack of chronic wound specific dressings – same bandages are used for both acute and chronic wounds [4,5]. There is a need for advanced wound dressings that would help to control the biochemical state of the wound and aid its healing processes [6].

Recently, notable advancement has occurred in the therapy of chronic wounds. Liu et al. [7] conducted a study where electrospun hyaluronic acid containing nanofibers were used to form *in situ* hydrogels in the wound bed. The authors concluded that the application of nanofibrous hydrogel on a chronic diabetic wound model resulted in accelerated wound healing [7]. In another study, the authors introduced an injectable and self-healing hydrogel for a wound treatment with a sustained release of active ingredient and proved its *in vivo* efficiency in a rat wound model showing its potential for human chronic wound therapy [8]. More recently, attempts have been made to accelerate the chronic wound healing processes by immunomodulation strategies, thus

* Corresponding author. Institute of Pharmacy, Faculty of Medicine, University of Tartu, Nooruse Str. 1, 50411, Tartu, Estonia.
*E-mail addresses:* arle.korkjas@ut.ee (A. Kõrkjas), kaarel.laar@gmail.com (K. Laar), ari.salmi@helsinki.fi (A. Salmi), joni.mk.makinen@helsinki.fi (J. Mäkinen), haeggstr@mappi.helsinki.fi (E. Hæggström), karin.kogermann@ut.ee (K. Kogermann), jyrki.heinamaki@ut.ee (J. Heinämäki), ivo.laidmae@ut.ee (I. Laidmäe).

https://doi.org/10.1016/j.jddst.2022.103935
Received 13 June 2022; Received in revised form 23 October 2022; Accepted 30 October 2022
Available online 2 November 2022

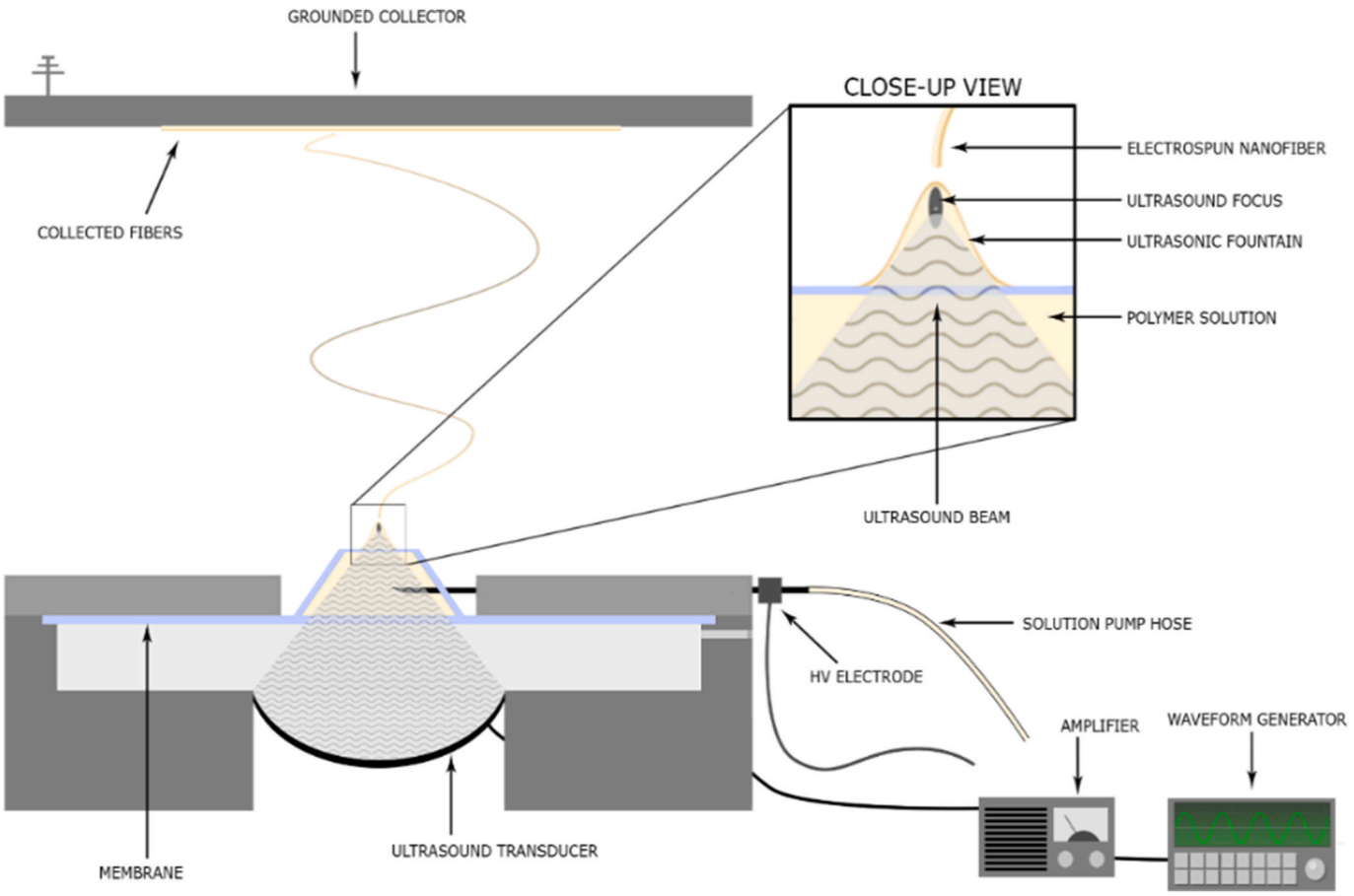


**Fig. 1.** Schematic of USES system equipped with an automated ultrasound signal generator for modulating the critical process parameters in real time during electrospinning.

showing how crucial the absence of infection in a chronic wound site is for faster wound healing [9]. Another approach often used for successful wound healing is tissue engineering, and today the use of autologous skin grafts is the most common approach to enhance chronic and hard-to-heal wound therapy [10]. Allogenic or xenogenic skin grafts can be considered for transplantation but their use is limited due to a high risk of rejection [10]. To overcome the lack of donor skin, medicine also uses artificial skin grafts. Artificial skin grafts are fabricated using biocompatible materials which include (but are not limited to) polymers such as (poly)ethylene oxide (PEO) and chitosan [10].

Conventional dressings for wound healing face many challenges. Conventional wound dressings are simple so ointments, gels and other materials are used for faster healing and to get the desired and needed effects, such as moisturising, anti-inflammatory, pain relieving effect [6]. Using conventional wound dressings together with multiple other materials and substances makes the wound dressing bulky and uncomfortable for the patient, impeding their everyday movements. A study conducted in 2009 found conventional dressings to be cost-ineffective since they required more often dressing changes [11]. Conventional scaffolds are unspecific systems which do not respect chronic wound properties. The proper fit of the scaffold in the wound bed is important for fast healing with few complications. A well-designed scaffold promotes cell proliferation and thus enhances the healing process [12]. For therapeutic efficiency it would be beneficial to integrate antimicrobial and anti-inflammatory agents with the wound dressing [13]. These challenges faced by conventional wound healing scaffolds create a demand for novel solutions; a demand that we address by using electrospun nanofibrous scaffolds designed for the treatment of chronic wounds.

These electrospun nanofiber scaffolds hold potential in biomedical applications as evident in a recent literature review [14]. Regardless, little advancement has been made on how the nanofibers are created. Conventional electrospinning equipped with a needle spinneret has been widely used in fabricating polymeric nanofibers, but this method is associated with some well-known limitations, such as a needle spinneret clogging and a limited production capacity [15]. Eventhough changing the process parameter(s) in a conventional electrospinning system is quite easy, the alteration of some key process parameters in real time involves a potential risk of electrospraying or dripping. For example, changing a flow rate can induce the polymeric solution too fast drying or dripping, thus modifying (or even destroying) the electrospun material. This in turn could limit electrospinning multilayered polymeric nanofibers with varying diameter.

The ability to modify nanofiber diameter on the fly gives us an opportunity to create advanced nanofiber materials with complex design. Such wound dressings and scaffolds could be used for advanced biomedical applications for specific healing and a personalized approach. The instant adjustment of fiber size and morphology as well as the generation of multilayered nanostructures could be an approach to fabricate advanced nanofibrous materials for wound therapy and tissue engineering applications. Engineered scaffolds with gradient structures have been shown to be superior to single-phase scaffolds in repairing osteochondral defects [16,17]. Fiber diameter also modulates neural stem cell differentiation and cell migration velocities [18,19]. Mechanical properties of the fibers (which correlate with fiber diameter) can guide cell response – differentiation, morphology, and migration [20–24].

To this regard, we developed a technique called ultrasound-

**Table 1**
Process parameters and their magnitude used in the electrospinning (USES) of multilayered PEO nanofiber mats.

| Process parameter | Magnitude (or range) applied in the USES process |
|---|---|
| Frequency (MHz) | 2.06 |
| Amplitude ($mV_{p-p}$) | 150/700[a] |
| Burst count (cycles) | 900/100[a] |
| Burst rate (Hz) | 150 |
| Flow rate (mL/h) | 0.5–2.0 |
| Distance (cm) | 25 |
| Voltage (kV) | 10 |
| Target voltage (kV) | −4.0 |
| Humidity (RH%) | 3–6 |
| Temperature (°C) | 30–33 |

[a] Amplitude was increased from 150 to 700 and burst count was decreased from 900 to 100 over one process period. Frequency of the change was once per second.

enhanced electrospinning (USES), which is an open liquid-surface needleless electrospinning method for producing polymeric nanofiber mats and nanofibrous scaffolds [25]. The technique employs an open vessel filled with a spinning solution, and utilizes focused ultrasound for creating a protrusion (Taylor cone) from which the nano- or microfibers are electrospun. The critical process parameters of a multivariate USES process can be changed and controlled in real-time during an electrospinning process. Changing critical parameters causes slight changes in the acoustic fountain [26]. In the present study, our main hypothesis was that USES can generate nanofibers with varying size, orientation, and layering properties through the modulation of process parameters in real time. It was expected that we could generate novel types of nanofibrous materials by layering the fibers of different size and size distributions throughout the electrospun nanofibrous mat, which could evidently advance wound healing and tissue regeneration [27]. Studies have shown that topographical factors including the diameter of the nanofibers can regulate cell growth [28].

The aims of the present study were (1) to investigate the potential of an open liquid-surface needleless USES method for fabricating multilayered polymeric nanofibrous mats intended for wound healing, tissue engineering, and drug delivery applications, (2) to understand the effects of process parameters (i.e., burst rate, burst count, amplitude, duty cycle and relative acoustic power) on the formation of nanofibers and fiber layers in the USES continuous manufacturing process, and (3) to investigate the potential solid-state changes in the materials used in the process. To accomplish this goal, the USES setup was implemented with an automated ultrasound signal generator and dynamic control system to modify on the fly the nanofiber formation.

## 2. Materials and methods

### 2.1. Materials

Polyethylene oxide, PEO (an average molecular weight of 900,000 Da) (Sigma-Aldrich Inc., U.S.A) was used as a mat forming polymer in the multilayered nanofibrous mats generated by the USES system. PEO was selected as a matrix forming polymer, since it is a safe and established water-soluble synthetic polymer enabling the use of aqueous solution in an electrospinning process. Purified water was used as a solvent for preparing the aqueous PEO solutions (4% w/v and 3.5% w/v) applied in the USES experiments.

### 2.2. Fabrication of nanofibers

An in-house open liquid-surface needleless USES method was used to generate nanofibers and multilayered nanofibrous mats (Fig. 1). The USES setup and method are described in detail in our previous paper [25]. In brief, the USES method is a needleless electrospinning system where ultrasound, that is focused on the liquid-air surface, generates a protrusion i.e., an acoustic fountain, that can serve as a base to form a Taylor cone. A high-voltage electrode is placed into the solution and a grounded collector plate is placed above the vessel containing the polymer solution. The resulting electric field enables the formation of nanofibers and jets the fibers from an acoustic fountain onto a grounded collector plate (Fig. 1). In USES, the critical ultrasound parameters (i.e., burst rate, burst count, amplitude) can be varied, and consequently used to govern the formation and final diameter of the nanofibers. Based on the input values duty cycle (DC) and relative acoustic power ($AP_{rel}$) can be calculated (see results).

In the present study, we implemented and tested an automated ultrasound signal generator to control and modify critical USES process parameters in real time during electrospinning, and subsequently to generate multilayered nanofibrous structures (Fig. 1). The acoustic fountain is generated by a focusing 2.06 MHz ultrasonic transducer. An arbitrary waveform generator (Agilent 33120A, Agilent Technologies, Incorporated, USA) drives a power amplifier (Kalmus Model 121C, Kalmus Engineering International, USA) that transmits the signal to the transducer. The relative humidity of a climate chamber that encases the USES setup was kept at 4–5% with a dehumidifier (COTES All-Round C30E-1.9 3 × 400V/50Hz PLUS, COTES A/S, Denmark). The waveform generator (Fig. 1) integrated in the USES system was programmed using the NI Labview NXG 4.0 software (National Instruments, Austin, TX, U.S.A). The present control system was applied to modulate the size of nanofibers during an electrospinning process and to generate multilayered polymeric nanofibrous structures.

The aqueous solution of PEO (3.5% w/v and 4% w/v) exhibited good electrospinnability. PEO allowed continuous spinning for extended periods (few hours) with little spraying and other erratic behaviour of the fiber formation at different USES parameter settings. PEO solution was thus selected for generating the multilayered nanofibrous mats. The USES process parameters and their magnitude are summarized in Table 1. The multi-layered PEO nanofibers were electrospun using both manual operation and an automated process monitoring/control system in USES process. We used a sine wave in all experiments. The nanofibers were electrospun from a PEO solution after a discernible acoustic fountain was established. The distance between the fountain and the collector plate was kept constant (25 cm). The ultrasound amplitude and burst count were altered. The processing time was 3–6 h, and the environmental temperature and humidity were controlled during the electrospinning process. Nanofibers were collected on a collector plate covered with an aluminum foil (Fig. 1).

### 2.3. Characterisation of nanofibers

Optical light microscopy (Magtex-T Dual Illum., Medline Scientific, United Kingdom) was used to visualize different layers in the electrospun nanofiber mats. An image was taken from the cross-section of the electrospun mat on aluminum foil.

Scanning electron microscopy, SEM (Zeiss EVO MA15, Jena, Germany) was applied to study the size and morphology of the nanofibers. Small pieces of samples were cut out of the electrospun nanofiber mat and placed onto special plates covered with carbon tape. The plates with samples were coated with an ultra-thin platinum layer prior to imaging. The SEM images were taken using three different magnifications (3000x, 15000x and 25000x). ImageJ software (Wayne Rasband, Bethesda, Maryland, USA) was used to measure the diameter of the nanofibers from the SEM images generated with a 15000x magnification. Approximately 100 measurements were taken from a single sample.

The presence of potential process-induced transformations of PEO in a needleless USES process were studied by Fourier transform infrared (FTIR) spectroscopy (IRPrestige 21, Shimadzu corporation, Kyoto, Japan) with a single reflection attenuated total reflection (ATR) crystal. The IR spectra of three different nanofiber and pure PEO powder samples were collected in a spectral range from 600 to 4000 $cm^{-1}$. Each

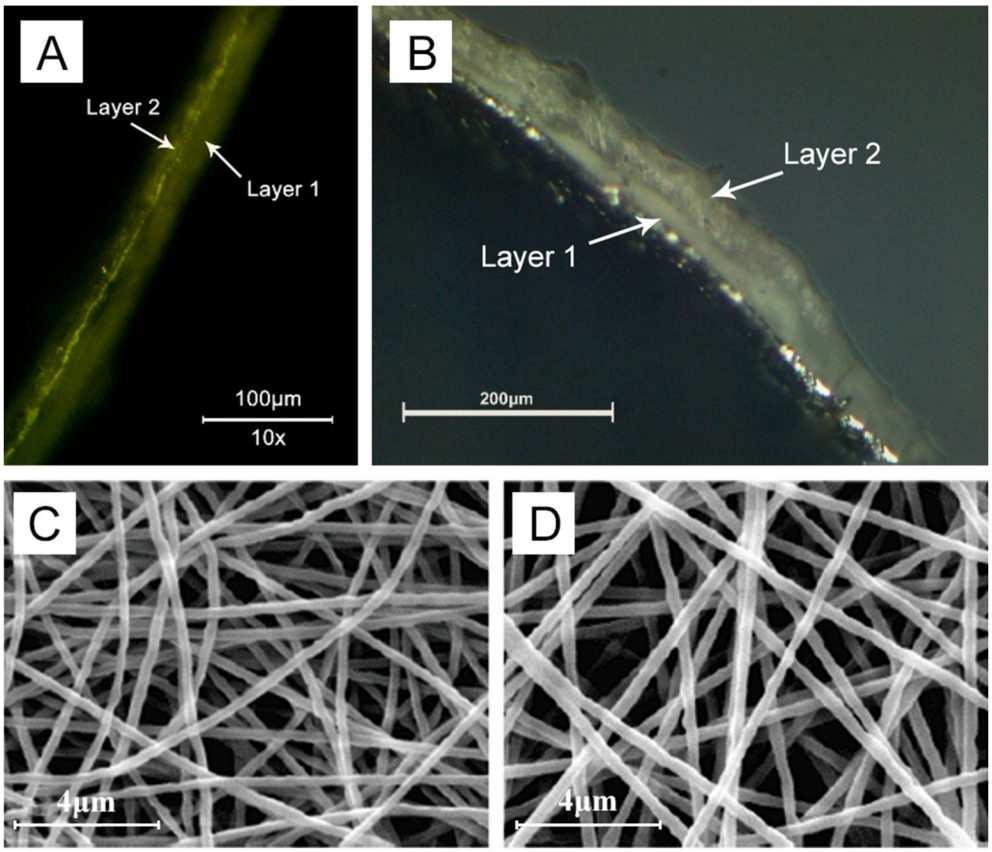


**Fig. 2.** Optical microscopy images (A–B) of the cross-section of bilayered ultrasound-enhanced electrospun PEO mats with a distinguishable boundary between the layers. Scanning electron micrographs of (C) the first layer („Layer 1“) and (D) the second layer („Layer 2“) in the nanofibrous mat shown in section (B).

**Table 2**
The effect of a stepwise change in an ultrasound burst rate on the diameter of multilayered PEO nanofibers in the USES process. Key: A = amplitude, BR = burst rate, BC = burst count, DC = duty cycle, $AP_{rel}$ = relative acoustic power, SD = standard deviation.

| Layers | Ultrasound parameter | | | | | Average fiber diameter (nm) n = 50 | SD |
|---|---|---|---|---|---|---|---|
| | A ($V_{p-p}$) | BR (Hz) | BC (cycles) | DC (%) | $AP_{rel}$ | | |
| 1 | 0.2 | 150 | 300 | 2.2 | 0.09 | 387 | 80 |
| 2 | 0.2 | 250 | 300 | 3.6 | 0.14 | 351 | 55 |
| 3 | 0.2 | 400 | 300 | 5.8 | 0.23 | 337 | 67 |
| 4 | 0.2 | 600 | 300 | 8.7 | 0.35 | 402 | 64 |
| 5 | 0.2 | 800 | 300 | 11.7 | 0.47 | 465 | 52 |
| 6 | 0.2 | 1000 | 300 | 14.6 | 0.58 | 421 | 34 |
| 7 | 0.2 | 1300 | 300 | 18.9 | 0.76 | 422 | 35 |
| 8 | 0.2 | 1800 | 300 | 26.2 | 1.05 | 474 | 56 |

sample was measured 40 times and the averages were calculated. The results were normalized and scaled, no other spectral pretreatments were applied.

### 2.4. Statistical analysis

Statistical analysis (one-way ANOVA) was carried out with a Microsoft Excel 2016 software (Microsoft Corporation, Redmond, Washington, U.S.) to determine whether there were statistically significant differences ($p < 0.05$) between the means of three or more independent groups. A Tukey-Kramer post-hoc test was conducted to determine if the groups differed from each other.

## 3. Results and discussion

### 3.1. Bilayered nanofibrous mats generated in the USES system

As first test with the USES system, we generated bilayered PEO nanofibrous mats by manually changing the ultrasound settings in the middle of the process. Optical light microscopy and SEM were used to visualize the two separate fibrous layers of the present nanofiber mats obtained from a 4% (w/v) aqueous PEO solution. Micrographs of two different bilayered PEO-based nanofiber mats are shown in Fig. 2.

As seen in Fig. 2, by using two different ultrasonic settings in USES process, it was possible to produce the polymeric nanofibrous mats with two distinguishable fiber layers. The test verified that the dimensions of the nanofibers in the separated layers can be modulated by changing the magnitude of the process parameters (ultrasound amplitude and burst count). Furthermore, it was evident that USES permits forming nanofibrous mats with decreasing or increasing fiber dimensions, and thus permits generating multilayered nanofibrous structures. To our best knowledge, no other needleless electrospinning method described in the literature to date is capable to spatiotemporally modify the topography or diameter of nanofibers at a real time.

Pelipenko et al. [29] reported that it is possible to modify the diameter of the nanofibers also in a traditional multivariate needle-based electrospinning. The material attributes affecting the formation and final properties of nanofibers include the type of polymer and the concentration of the polymer solution used in electrospinning. In addition, several process parameters and ambient parameters affect the fiber thickness and morphology: voltage applied in the process, tip to collector distance, flow rate of the solution, relative humidity and temperature in the electrospinning chamber [30]. More recently, Sebe et al. [31] generated multilayered nanofiber mats by using needle-based

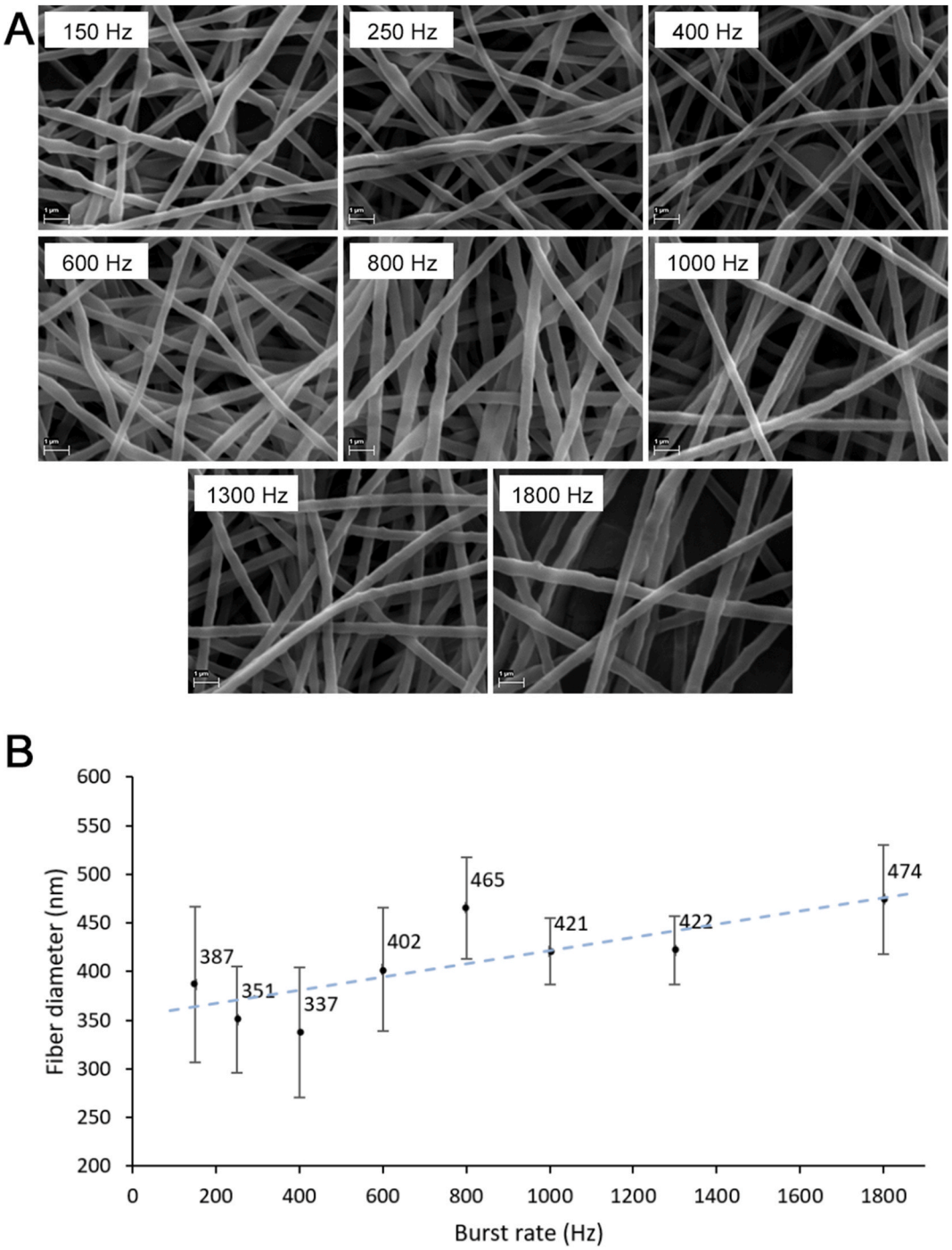


**Fig. 3.** (A) Scanning electron microscopy images of eight consecutive fiber layers of PEO nanofiber mats generated in the USES process. The stepwise increase of ultrasound burst rate (BR) ranged from 150 Hz to 1800 Hz (reference is also made to Table 2). (B) The effect of stepwise change in ultrasound BR on the average diameter of PEO nanofibers (n = 50) in eight consecutive fiber layers generated in the USES process. Error bars represent standard deviation (SD). Blue dotted line shows the upwards trend of the fiber diameter increase as the burst rate is increased. (For interpretation of the references to colour in this figure legend, the reader is referred to the Web version of this article.)

electrospinning for delivering colistin sulfate through a body surface. The effect of alternate layer arrangements on the drug-release profiles was also investigated to plan for controlled topical drug release from fibrous scaffolds.

While it is possible to make changes to the nanofiber diameter with a traditional needle-based electrospinning, the real-time change in the level(s) of key process parameters under the process is difficult, and such changes could affect already collected material. The alteration of process parameters could greatly affect also the spinnability of a polymer solution. Moreover, the time period for such shift is rather long for enabling an instantaneous fiber change in a needle-based conventional electrospinning. With USES instant changes of the process parameters are possible. The present stepwise change of the critical process parameters during the USES process enables creating nanofibrous systems which is challenging with traditional electrospinning [26].

**Table 3**
The effect of burst count on the diameter of PEO nanofibers in USES. Key: A = amplitude, BR = burst rate, BC = burst count, DC = duty cycle, $AP_{rel}$ = relative acoustic power, SD = standard deviation.

| | Ultrasound parameters used | | | | | | |
|---|---|---|---|---|---|---|---|
| Layers | A ($V_{p-p}$) | BR (Hz) | BC (cycles) | DC (%) | $AP_{rel}$ | Average fiber diameter (nm) n = 50 | SD |
| 1 | 0.15 | 150 | 1200 | 8.7 | 0.20 | 478 | 55 |
| 2 | 0.15 | 150 | 1400 | 10.2 | 0.23 | 402 | 35 |
| 3 | 0.15 | 150 | 1600 | 11.7 | 0.26 | 489 | 62 |
| 4 | 0.18 | 180 | 1800 | 15.7 | 0.51 | 428 | 55 |
| 5 | 0.18 | 180 | 2000 | 17.5 | 0.57 | 408 | 34 |
| 6 | 0.18 | 180 | 2200 | 19.2 | 0.62 | 429 | 45 |
| 7 | 0.18 | 180 | 2400 | 21.0 | 0.68 | 455 | 58 |
| 8 | 0.18 | 180 | 2600 | 22.7 | 0.74 | 423 | 56 |
| 9 | 0.1 | 100 | 4500 | 21.8 | 0.22 | 383 | 54 |
| 10 | 0.1 | 100 | 6500 | 31.6 | 0.32 | 384 | 33 |
| 11 | 0.1 | 100 | 10000 | 48.5 | 0.49 | 307 | 22 |

### 3.2. Multilayered nanofibrous mats generated with the USES system

#### 3.2.1. Effect of burst rate on the formation and diameter of layered nanofibers

We investigated the impact of a stepwise change in two independent USES process parameters (i.e., ultrasound burst rate or burst count) on the fiber diameter in the multilayered nanofibrous mats. Nanofiber mats with different numbers of layers were prepared for investigating the effect of USES parameters. The effects of a gradual change in burst rate (BR) on the diameter of multilayered PEO nanofibers in USES process are presented in Table 2 and (Fig. 3). The BR was increased for every subsequent fiber layer that was generated, and the total number of nanofiber layers generated was eight. Ultrasound amplitude and distance to the collector plate was adjusted slightly to stabilize the electrospinning process. The magnitude of other process parameters in the USES system were kept constant (excluding the two dependent process parameters ultrasound duty cycle and relative acoustic power which varied with the change in two independent process parameters).

As shown in Table 2 and (Fig. 3), the increase in BR had an effect on the formation and thickness of the PEO nanofibers generated by USES. As BR was increased stepwise from 150 Hz to 1800 Hz, the average fiber size increased from 387 nm to 474 nm, respectively. The smallest average fiber diameter (337 ± 67 nm), was found in the third layer (generated at 400 Hz) instead of the first fiber layer (generated at the lowest BR of 150 Hz). The final eighth fiber layer generated at 1800 Hz consisted of nanofibers with the highest average fiber diameter of 474 ± 56 nm. In the present study, we used DC levels in the range of 2.2% and 26.2%, suggesting that there is still room to increase the BR for generating the nanofibers with higher fiber diameter, if the ultrasonic fountain is stable enough.

#### 3.2.2. Effect of burst count on the formation and diameter of layered nanofibers

The effects of stepwise increased ultrasound BC on the fiber diameter

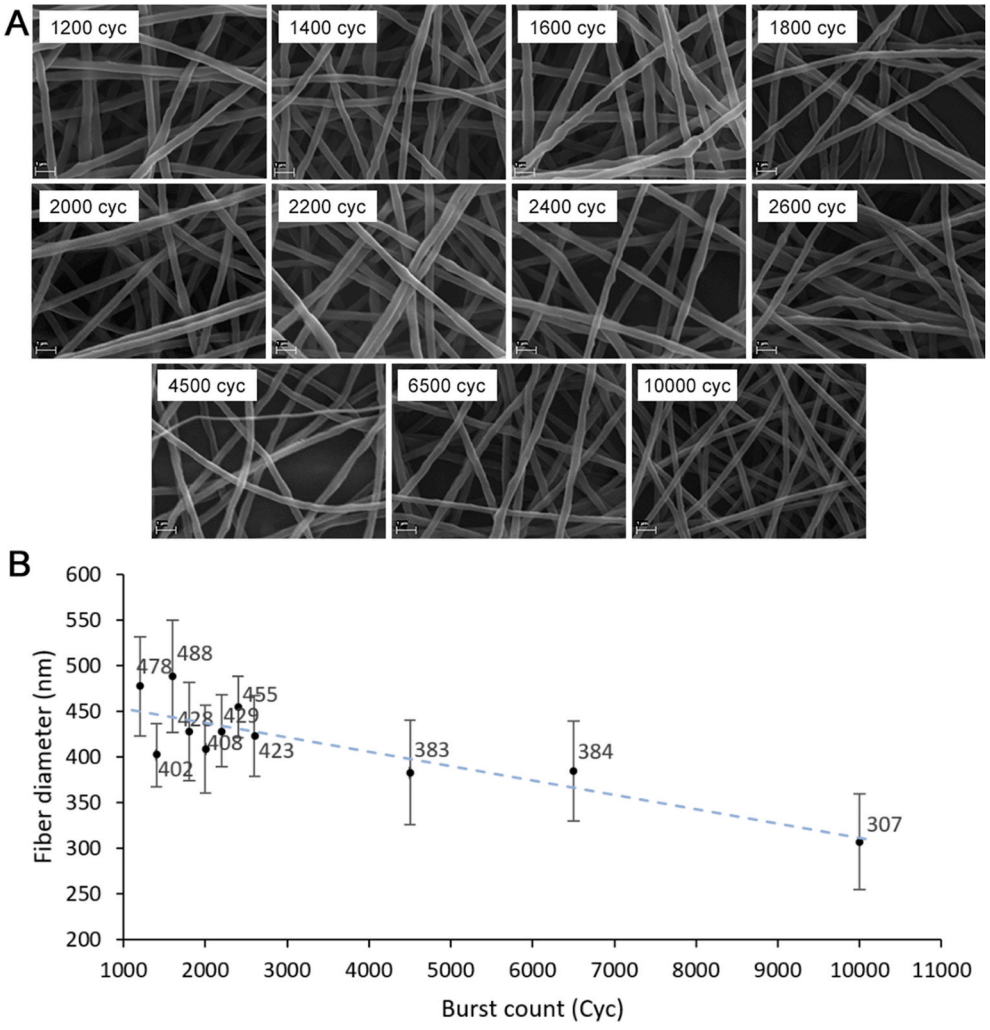


**Fig. 4.** (A) Scanning electron microscopy images of eleven consecutive fiber layers of PEO nanofiber mats generated in an USES machine. The stepwise increased ultrasound burst count (BC) ranged from 1200 cycles to 10000 cycles (reference is also made to Table 3). (B) The effect of a stepwise change in BC on the diameter of PEO nanofibers (n = 50) in the eleven consecutive fiber layers generated in the USES process. Error bars represent one standard deviation (SD). Blue dotted line shows a downward trend of the nanofiber size when burst count is increased. (For interpretation of the references to colour in this figure legend, the reader is referred to the Web version of this article.)

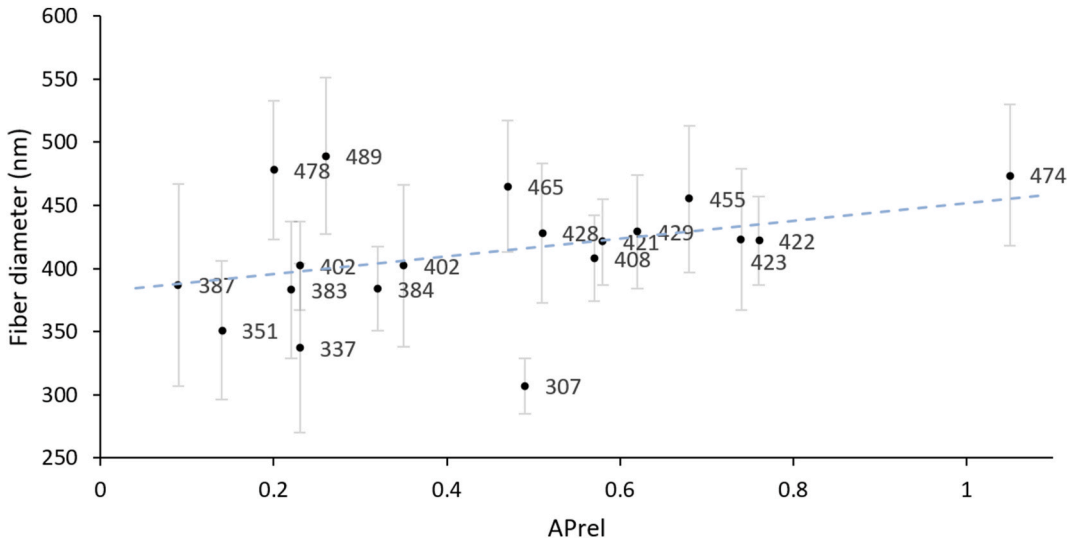


**Fig. 5.** The effect of relative acoustic power ($AP_{rel}$) values on the diameter of PEO nanofibers (n = 50) in 19 (Tables 2 and 3 samples combined) fiber layers generated in the USES process. Error bars represent one standard deviation (SD). Blue dotted line shows an upwards trend of fiber diameter as $AP_{rel}$ is increased. (For interpretation of the references to colour in this figure legend, the reader is referred to the Web version of this article.)

**Table 4**
The combined effect of duty cycle and relative acoustic power on the diameter of layered PEO nanofibers in USES process. Key: A = amplitude, BR = burst rate, BC = burst count, DC = duty cycle, $AP_{rel}$ = relative acoustic power, SD = standard deviation.

| | Ultrasound parameters used | | | | | | |
|---|---|---|---|---|---|---|---|
| Layers | A ($V_{p-p}$) | BR (Hz) | BC (cycles) | DC (%) | $AP_{rel}$ | Average fiber diameter (nm) n = 50 | SD |
| 1 | 0.30 | 250 | 155 | 1.8 | 0.16 | 184 | 26 |
| 2 | 0.30 | 250 | 200 | 2.4 | 0.22 | 150 | 26 |
| 3 | 0.30 | 250 | 268 | 3.2 | 0.29 | 147 | 29 |
| 4 | 0.30 | 250 | 376 | 4.6 | 0.41 | 134 | 30 |
| 5 | 0.30 | 250 | 567 | 6.9 | 0.62 | 141 | 38 |
| 6 | 0.30 | 250 | 950 | 11.5 | 1.04 | 135 | 32 |

in 11 consecutive layers generated with USES was investigated similarly to the effects of BR by increasing the BC for each sample (fiber layer). The results of these experiments are shown in Table 3 and (Fig. 4). Other parameters in the USES system were unchanged apart from minor corrections to amplitude and collector plate distance.

As seen in (Fig. 4A), all fiber layers (generated by stepwise increases in the BC levels from 1200 cycles to 10000 cycles), consisted of nanofibers with a uniform size and surface morphology, and the absence of beads (defects). Increasing BC reduced the average diameter of nanofibers in the fiber layers generated by USES. As BC was increased from 1200 cycles to 10000 cycles, the average diameter of nanofibers decreased by 170 nm (Table 3 and Fig. 4B). Applying BC above 4500 cycles resulted in the average diameter of nanofibers (fiber layers) ranging from 300 nm to 400 nm. Even though there was a downward trend in the fiber thickness with increasing BC, this trend was not monotoneus. Perhaps surprisingly, the thickest nanofibers (478–489 nm in diameter) were found in the first fiber layer (generated at 1200 cycles) and the third fiber layer (at 1600 cycles), whereas the thinnest nanofibers (307 nm in diameter) were detected in the final (eleventh) fiber layer (at 10000 cycles) (Table 3).

Having BC less than 1200 cycles was not possible with USES when trying to keep the amplitude and BR low since the ultrasonic fountain on top of the solution was either unstable or did not appear at all. Application of BC above 10000 cycles is technically possible, and this could enable us to fabricate even thinner polymeric nanofibers. Minor changes in amplitude (A) and BR were necessary to stabilize the ultrasonic cone on top of the solution in the vessel. Note that DC and $AP_{rel}$ also changed when making these changes. Due to these changes the effect of the BC decrease on the formulation of nanofibers is not a clear-cut. The effect can be observed when comparing layers with an A value of 0.15 and 0.1. While the $AP_{rel}$ stays similar we increased the BC considerably and managed to generate nanofibers with lower and lower thickness as BC increased. In these experiments, we used a DC in the range of 8.7% and 48.5%, thus suggesting that there is still room to increase BC for generating thinner nanofibers. Fig. 5 shows the nanofiber diameter at different $AP_{rel}$ values obtained in previous BC and BR tests.

In the present USES system, ultrasound has a specific focal point which needs to be taken into account in electrospinning. Furthermore, the liquid surface level in the vessel needs to be manually controlled and adjusted. These facts could explain the slight deviations in the present results as the ultrasonic fountain is greatly affected by minor changes in the ultrasound focus point and by the liquid surface level in the vessel. USES is a multivariate system in which a number of factors (such as pulse repetition frequency and its effect on the viscoelasticity of a polymer solution) can affect the outcome of the process. Therefore, further studies are needed to identify the critical process factors affecting the fiber size and to make these changes in a controlled manner.

### *3.2.3. The impact of duty cycle and relative acoustic power on the diameter of layered nanofibers*

We investigated the impact of (DC) and relative acoustic power ($AP_{rel}$) as a combined process parameter on the diameter of PEO nanofibers in six consecutive fiber layers generated by USES. In this test set we used 3.5% (w/v) PEO solution, which plays a role in generating thinner fibers overall. The results are summarized in Table 4 and (Figs. 6–8). The DC was calculated using Eq (1).

$$DC\ (\%) = \frac{PW}{T} * 100 \qquad \text{[Eq. 1]}$$

where PW is the impulse period (1/f * BC), and T is the impulse repetition period (1/BR).

The relative acoustic power can be estimated using Eq (2).

$$AP_{rel} \approx A^2 * DC \qquad \text{[Eq. 2]}$$

Table 4 summarizes the magnitude of the process parameters and the

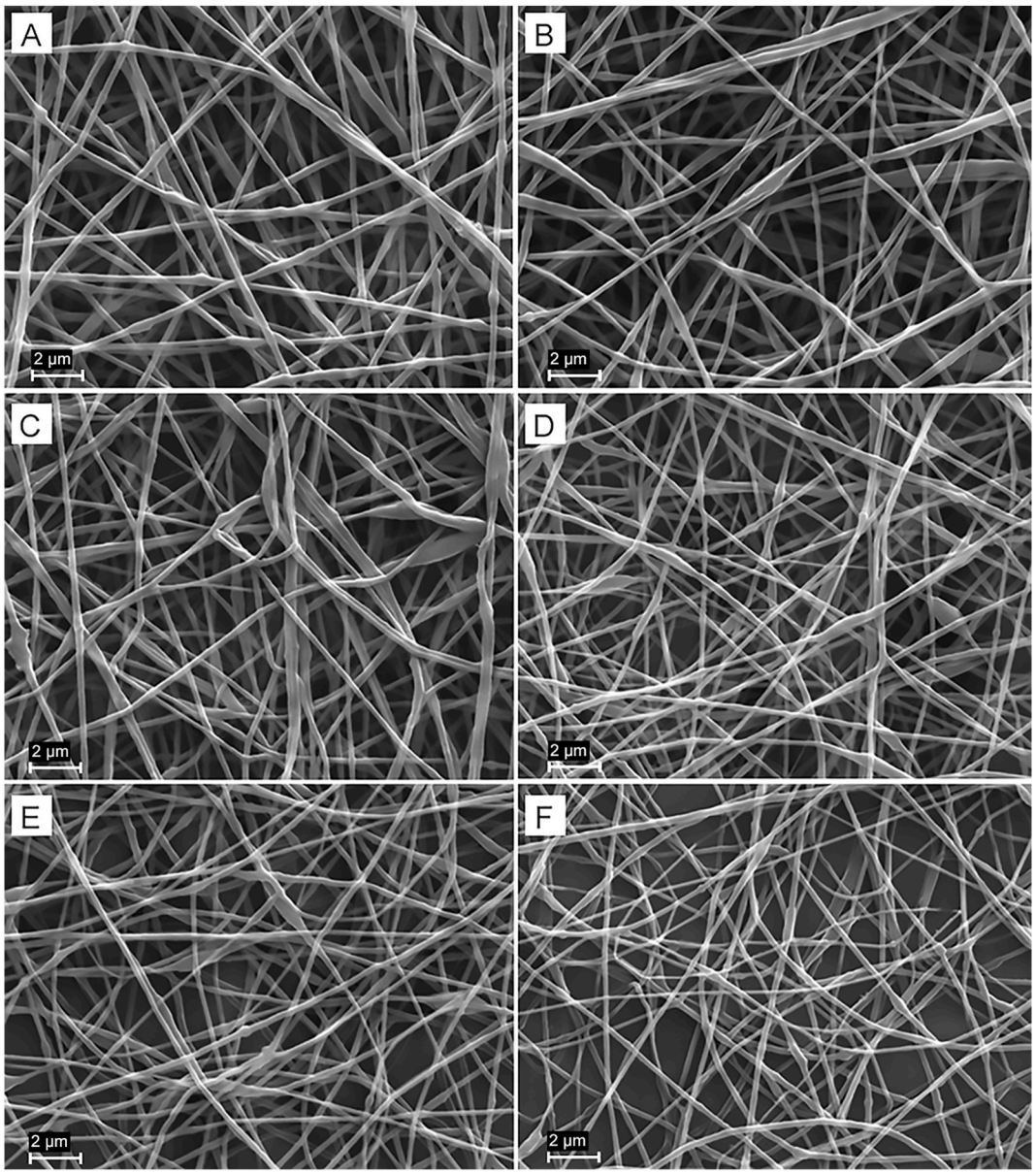


**Fig. 6.** Scanning electron microscopy images of PEO nanofibers generated in USES process (reference is also made to Table 4). Magnification 15000×. Key: (A) Layer 1, (B) Layer 2, (C) Layer 3, (D) Layer 4, (E) Layer 5, (F) Layer 6.

average diameter of the nanofibers in six consecutive fiber layers generated by USES. The average fiber diameter in six fiber layers was 134–184 nm, and the ANOVA analysis (Table 5) showed statistically significant differences in the diameter of nanofibers in these six consecutive fiber layers ($p < 0.05$). The amplitude A ($V_{p\text{-}p}$) and BR were kept constant, whereas BC was stepwise increased during electrospinning of the consecutive fiber layers. As seen in Table 4, BC affected DC and $AP_{rel}$ which both increased with increasing BC. Note that the last fiber layer was electrospun at the highest $AP_{rel}$ value that did not affect the ultrasonic fountain stability. The nanofibers electrospun in the first fiber layer exhibited the largest average diameter (184 ± 26 nm), and the nanofibers electrospun in the final (6th layer) and fourth (4th) fiber layers exhibited the smallest average diameter (135 ± 32 nm and 134 ± 30 nm, respectively).

Fig. 6 presents SEM images of PEO nanofibers in six consecutive layers generated by the USES process. Here DC and $AP_{rel}$ values were altered through increasing BC at regular intervals. The nanofibers in the different fiber layers were thin (less than 200 nm in average diameter) and uniform in thickness. Few artefacts such as droplets, beads and thin web-structures were observed in the SEM micrographs, thus indicating a controlled and stable electrospinning process. Distribution of nanofiber diameters with their respective average diameter is illustrated on Fig. 7.

As DC and $AP_{rel}$ were increased, the change in fiber diameter within the last three layers (4–6) was negligible. No statistically significant differences were found between the nanofiber size of the last three fiber layers (Table 5). A slight decrease in fiber diameter was observed when DC and $AP_{rel}$ increased with increasing BC levels ranging from 1.8% to 4.6% and from 0.16 to 0.41, respectively (i.e., within the fiber layers 1–4). The diameter of the nanofibers differed by 50 nm. The decrease in nanofiber size was statistically significant ($p < 0.05$) within the fiber layers 1–4 (Table 5). Statistically significant differences in nanofiber size were also found between fiber layers 1 and 6, and between fiber layers 6 and 2. The diameter of nanofibers in the first fiber layer was statistically different ($p < 0.05$) from the nanofiber diameters in all other fiber layers. The nanofibers having the largest average diameter (1st fiber layer) were electrospun with 15% of the $AP_{rel}$ that was used to make on

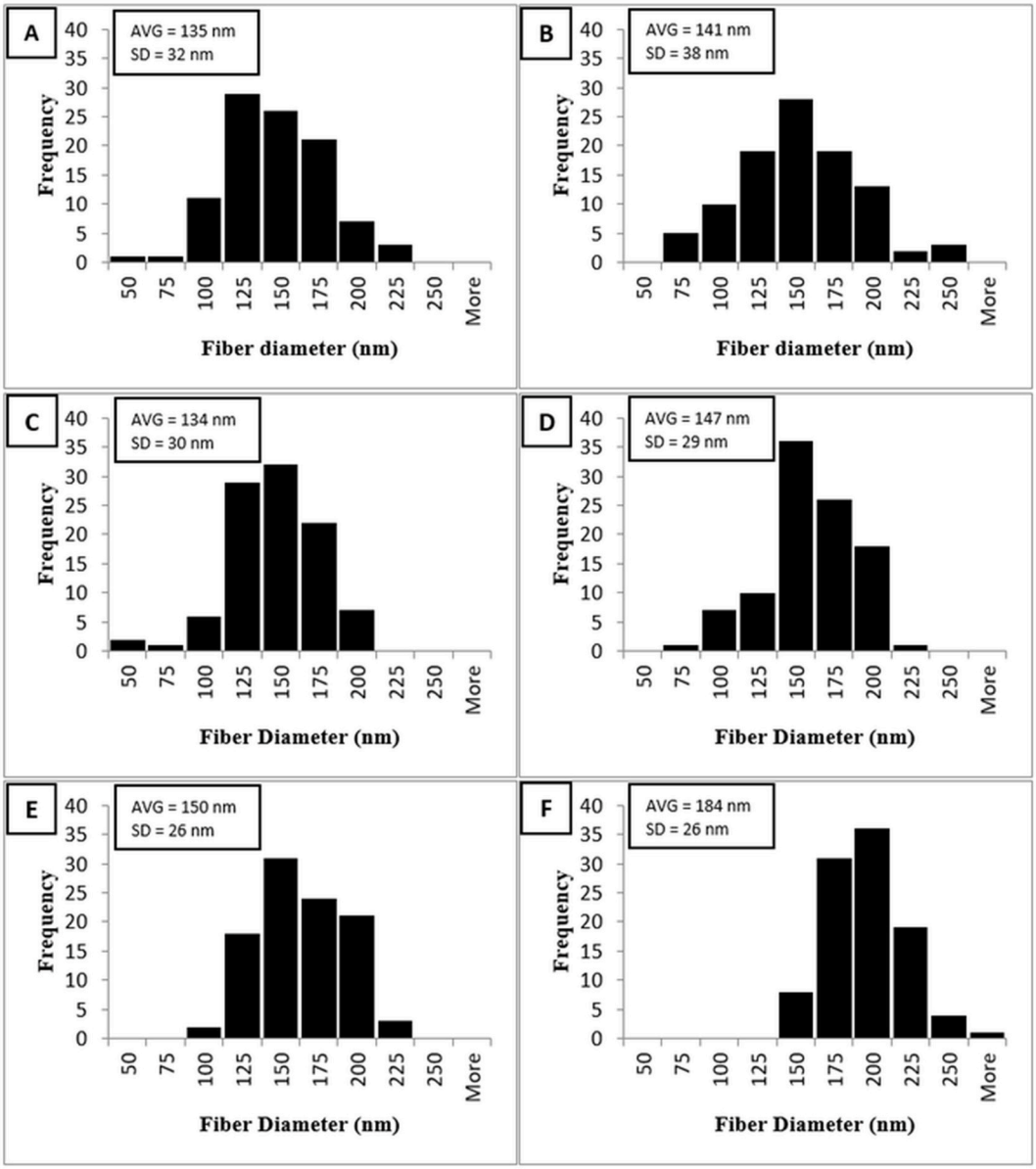


**Fig. 7.** The fiber diameter (nm) distribution (n = 100) of six consecutive fiber layers. Key: (A) Layer 1, (B) Layer 2, (C) Layer 3, (D) Layer 4, (E) Layer 5, (F) Layer 6.

average 49 nm thinner nanofibers in the last layer (6th fiber layer).

### 3.2.4. *Effect of USES on the physicochemical structure of layered nanofibers*

FTIR spectroscopy analysis was carried out on the nanofiber samples generated by USES and the spectra were compared to the one obtained with a pure PEO powder sample. No significant peak shifts nor intensity differences were observed in the FTIR spectra when comparing the spectra of USES nanofibers and pure PEO (Fig. 8), hence highlighting that PEO did not change its crystallinity during electrospinning from aqueous solution. Both samples showed the characteristic IR peak for PEO near 2900 $cm^{-1}$ which is assigned to C–H stretching [32]. The other characteristic peaks of PEO are at 961 $cm^{-1}$, 1060 $cm^{-1}$, 1091 $cm^{-1}$ (the highest peak) and 1149 $cm^{-1}$ which are assigned to C–O–C stretching vibration. The C–H deformation modes are shown at 1342 $cm^{-1}$ and 1361 $cm^{-1}$.

According to the literature, the structural changes of PEO were observed even after a short storage time [33]. In our work, we verified that the USES process intrinsically does not cause any structural changes to a PEO-based formulation. Further research work, however, is needed to find out the potential of structural changes of the present multilayered PEO nanofibers under a short-term and/or long-term storage stability test.

### 3.2.5. *The potential of using USES to fabricate multilayered nanofiber mats*

The number of scientific papers published on the USES method is limited, and consequently, little is known about the impact of the USES process parameters in fabricating nanofibers and nanofiber mats. An open liquid-surface USES system was introduced by Nieminen et al. [25], and they used PEO as a carrier polymer in their work with a slightly lower polymer concentration level than the one we used in the current study (3% *vs* 4%, respectively).

The USES method applies a high-intensity focused ultrasound to induce a local acoustic radiation pressure to the surface of the polymer solution (Fig. 1). A localized impact of ultrasound on the polymer solution-air interface generates a protrusion and then a fiber jet under a high electric field potential between the liquid surface and collector plate. The underlying effects on an electrospinning solution and fiber formation at the proximity of an ultrasound fountain, include e.g., acoustic radiation force, capillary waves, cavitation, acoustic streaming

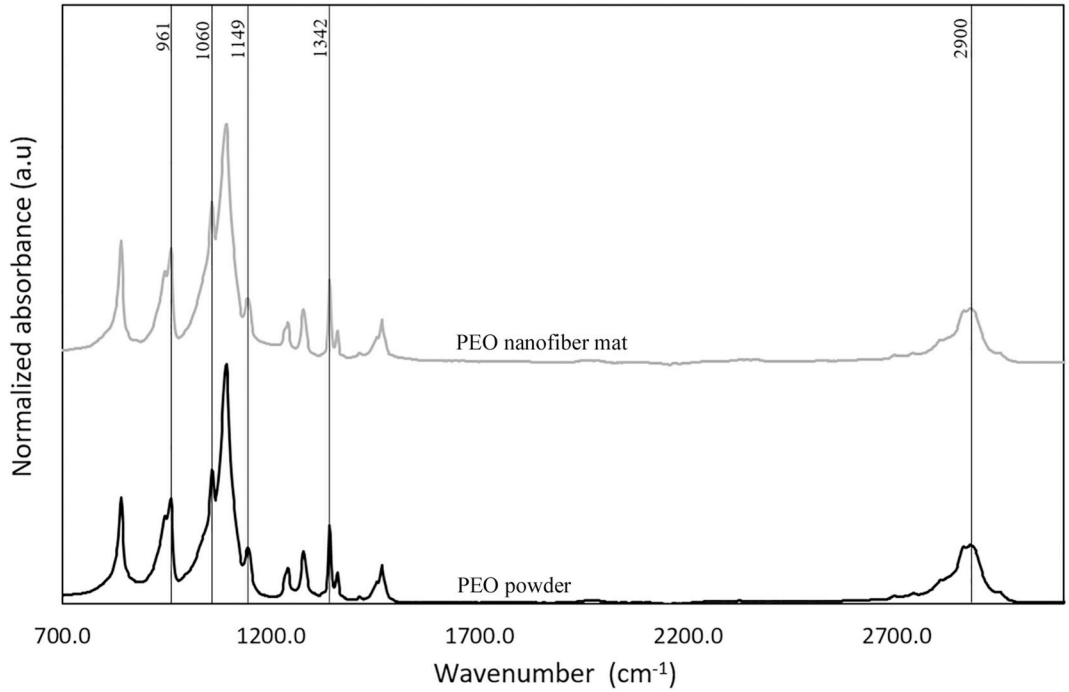


**Fig. 8.** Fourier transform infrared (FTIR) spectra of a PEO nanofiber mat generated with the USES system, and pure PEO powder for comparison. The FTIR spectra are normalized and scaled.

**Table 5**
Summary of the statistical analysis (ANOVA and Tukey-Kramer *post-hoc* test) comparing the average nanofiber diameter of different consecutive fiber layers generated with the USES process (reference is also made to Table 4). Key: NS = non-significant statistical difference; * = statistical significant difference ($p < 0.05$); na = not applicable.

| Layer number | 1 | 2 | 3 | 4 | 5 | 6 |
|---|---|---|---|---|---|---|
| 1 | na | | | | | |
| 2 | * | na | | | | |
| 3 | * | NS | na | | | |
| 4 | * | * | * | na | | |
| 5 | * | NS | NS | NS | na | |
| 6 | * | * | NS | NS | NS | na |

and thermal effects [25]. Since acoustic radiation force and electric field density are concentrated at the tip of the ultrasound fountain, it is evident that by altering the USES process parameters affecting this point, we could rapidly alter the formation and dimensions of nanofibers.

Nieminen et al. [25] found that an increase in total acoustic power during electrospinning resulted in the formation of thinner nanofibers. This finding is supported by our current work which shows generation of thicker nanofibers as a function of reduced $AP_{rel}$. Surprisingly, our first test series showed an opposite effect. It seems that the fiber diameter is not strictly related to the acoustic power suggesting that other process parameters such as BC and BR can be more descriptive than just $AP_{rel}$ on the formation of nanofibers with USES. Furthermore, $AP_{rel}$ is an estimated parameter that is modified by amplitude, burst rate, and burst count, and thus there are multiple ways of increasing or decreasing this value.

In our recent study, we showed that the diameter of nanofibers increased with increasing BC [26], which disagrees with the results obtained in our current study. The contradictory results might be due to the different polymer solution used in these two studies. In our previous study, we used a 3% aqueous polymer solution of PEO and chitosan (7:3). Moreover, many process variables and relative humidity (RH) in the USES chamber were different in these two studies, thus making the process conditions and results incomparable. For example, a high RH in the USES chamber makes it hard to evaporate solvent, which in turn affects the thickness of nanofibers. Consequently it is reasonable to control RH in the USES chamber, and for that we upgraded the USES system with an add-on humidity control system, which kept the humidity low.

The performance of USES should next be tested with different carrier polymers and solvent systems, since these materials may act differently in the system. In this study, we used PEO as a water-soluble model polymer due to its ease of use in our system and for ecological reasons. PEO has shear-thinning rheological properties, which should not be overlooked [34]. As the fountain is generated by rapid pulses of ultrasound on the top of a vessel in an open liquid-surface USES process, the liquid (polymer solution) is constantly being moved up and down as the ultrasonic wave is turned on and off in a rapid manner. This affects the state and behavior of a shear-thinning PEO solution, by making it thinner and less viscous. The viscosity of the solution directly affects the formation of nanofibers in electrospinning, and this should be considered [35]. Therefore, more studies are necessary to verify how rheological properties of different polymer solutions affect the uniformity of nanofiber mats produced with USES.

## 4. Conclusions

An ultrasound-enhanced electrospinning was used to generate bilayered and multilayered nanofibrous mats. The present USES method enables to induce rapid spatiotemporal changes to polymeric nanofibers „on fly“, thus providing improvement over the state-of-the-art electrospinning methods. The fabrication of multilayered nanofibrous mats was further developed by stepwise altering the critical process parameters in the USES system to modify the nanofiber size in the different fiber layers. PEO was used as a water-soluble carrier polymer in the multilayered nanofibrous mats. In the first experiments, we increased burst rate (BR) to electrospin multilayered nanofiber mats with eight individual nanofiber layers in which the fiber thickness was increased layer by layer. The second set of nanofiber mats was electrospun similarly, but instead

of increasing BR, the burst count (BC) was increased over eleven fiber layers. The multilayered nanofiber mats showed a decreasing trend in nanofiber thickness over the eleven fiber layers electrospun. The third set of experiments was conducted to investigate the effects of duty cycle (DC) and relative acoustic power ($AP_{rel}$) on the formation and nanofiber size of the multilayered nanofiber mats (6 layers). The results suggested that with decreasing DC the size of the nanofibers increased in the fiber layers. FTIR spectroscopy verified that no process induced transformations were induced when electrospinning PEO polymer with USES. It is evident that focused ultrasound alters the rheological properties of a polymer solution under electrospinning, and consequently, further research work is needed to find out the effect of this phenomen on an USES process. Based on the results obtained, we believe that USES could hold promise in fabricating multilayered (gradient) nanofibrous structures for wound healing and tissue engineering applications.

## Author statements

**Arle Kõrkjas:** Investigation, Methodology, Formal analysis, Writing - Original Draft, Writing - Review & Editing, Visualization. **Kaarel Laar:** Investigation, Formal analysis, Writing - Review & Editing. **Ari Salmi:** Conceptualization, Resources, Writing - Review & Editing, Supervision, Funding acquisition. **Joni Mäkinen:** Methodology, Writing - Review & Editing. **Edward Hæggström:** Conceptualization, Writing - Review & Editing, Supervision, Funding acquisition. **Karin Kogermann:** Conceptualization, Methodology, Writing - Review & Editing, Supervision, Funding acquisition. **Jyrki Heinämäki:** Conceptualization, Methodology, Writing - Review & Editing, Supervision, Funding acquisition. **Ivo Laidmäe:** Conceptualization, Methodology, Investigation, Resources, Writing - Review & Editing, Visualization, Supervision, Project administration.

## Declaration of competing interest

The authors declare the following financial interests/personal relationships which may be considered as potential competing interests: Ivo Laidmae has patent #EP3274491B1 issued to University of Helsinki. Ari Salmi has patent #EP3274491B1 issued to University of Helsinki. Jyrki Heinamaki has patent #EP3274491B1 issued to University of Helsinki. Edward Haeggstrom has patent #EP3274491B1 issued to University of Helsinki.

## Data availability

Data will be made available on request.

## Acknowledgements

This work is supported by the Estonian Research Council projects IUT 34-18, PRG1507 and PRG712. The Estonian Ministry of Education and Research is acknowledged for a financial support. The present study was also supported by the "Acouspin - Accelerated wound healing" project funded by the Business Finland. Special thanks to Prof Kalle Kirsimäe, MSc Marian Külaviir and MSc Georg-Marten Lanno for the help with SEM images.

## References

[1] K. Järbrink, G. Ni, H. Sönnergren, A. Schmidtchen, C. Pang, R. Bajpai, J. Car, Prevalence and incidence of chronic wounds and related complications: a protocol for a systematic review, Syst. Rev. 5 (2016) 1–6, https://doi.org/10.1186/S13643-016-0329-Y.

[2] W.H. Eaglstein, V. Falanga, CHRONIC WOUNDS, vol. 77, Surgical Clinics of North America, 1997, pp. 689–700, https://doi.org/10.1016/S0039-6109(05)70575-2.

[3] N.X. Landén, D. Li, M. Ståhle, Transition from inflammation to proliferation: a critical step during wound healing, Cell. Mol. Life Sci. 73 (2016) 3861–3885, https://doi.org/10.1007/S00018-016-2268-0.

[4] S. Gupta, S. Sagar, G. Maheshwari, T. Kisaka, S. Tripathi, Chronic Wounds-Magnitude, Socioeconomic Burden and Consequences, New Delhi, 2021. www.woundsasia.com.

[5] M. Mahmoudi, L.J. Gould, Opportunities and challenges of the management of chronic wounds: a multidisciplinary viewpoint, Chron. Wound Care Manag. Res. 7 (2020) 27–36, https://doi.org/10.2147/CWCMR.S260136.

[6] P. Zahedi, I. Rezaeian, S.O. Ranaei-Siadat, S.H. Jafari, P. Supaphol, A review on wound dressings with an emphasis on electrospun nanofibrous polymeric bandages, Polym. Adv. Technol. 21 (2010) 77–95, https://doi.org/10.1002/PAT.1625.

[7] S. Liu, Q. Zhang, J. Yu, N. Shao, H. Lu, J. Guo, X. Qiu, D. Zhou, Y. Huang, Absorbable thioether grafted hyaluronic acid nanofibrous hydrogel for synergistic modulation of inflammation microenvironment to accelerate chronic diabetic wound healing, Adv Healthc Mater 9 (2020), 2000198, https://doi.org/10.1002/ADHM.202000198.

[8] Z. Qian, H. Wang, Y. Bai, Y. Wang, L. Tao, Y. Wei, Y. Fan, X. Guo, H. Liu, Improving chronic diabetic wound healing through an injectable and self-healing hydrogel with platelet-rich plasma release, ACS Appl. Mater. Interfaces 12 (2020) 55659–55674, https://doi.org/10.1021/ACSAMI.0C17142.

[9] P. Heydari, M. Kharaziha, J. Varshosaz, S.H. Javanmard, Current knowledge of immunomodulation strategies for chronic skin wound repair, J. Biomed. Mater. Res. B Appl. Biomater. 110 (2022) 265–288, https://doi.org/10.1002/JBM.B.34921.

[10] A. Przekora, A concise review on tissue engineered artificial skin grafts for chronic wound treatment: can we reconstruct functional skin tissue in vitro? Cells 9 (2020) 1622, https://doi.org/10.3390/CELLS9071622.

[11] W.G. Payne, J. Posnett, O. Alvarez, M. Brown-Etris, G. Jameson, R. Wolcott, H. Dharma, S. Hartwell, D. Ochs, A prospective, randomized clinical trial to assess the cost-effectiveness of a modern foam dressing versus a traditional saline gauze dressing in the treatment of stage II pressure ulcers, Ostomy/Wound Manag. 55 (2009) 50–55. http://www.ncbi.nlm.nih.gov/pubmed/19246785.

[12] M.R. MacEwan, S. MacEwan, T.R. Kovacs, J. Batts, What makes the optimal wound healing material? A review of current science and introduction of a synthetic nanofabricated wound care scaffold, Cureus 9 (2017), https://doi.org/10.7759/CUREUS.1736.

[13] I. Negut, G. Dorcioman, V. Grumezescu, Scaffolds for wound healing applications, Polymers 12 (2020) (2010), https://doi.org/10.3390/POLYM12092010.

[14] S. Chen, B. Liu, M.A. Carlson, A.F. Gombart, D.A. Reilly, J. Xie, Recent advances in electrospun nanofibers for wound healing, Nanomedicine 12 (2017) 1335–1352, https://doi.org/10.2217/NNM-2017-0017.

[15] I. Partheniadis, I. Nikolakakis, I. Laidmäe, J. Heinämäki, A mini-review: needleless electrospinning of nanofibers for pharmaceutical and biomedical applications, Processes 8 (2020) 673, https://doi.org/10.3390/PR8060673.

[16] S. Ansari, S. Khorshidi, A. Karkhaneh, Engineering of gradient osteochondral tissue: from nature to lab, Acta Biomater. 87 (2019) 41–54, https://doi.org/10.1016/J.ACTBIO.2019.01.071.

[17] H. Kang, Y. Zeng, S. Varghese, Functionally graded multilayer scaffolds for in vivo osteochondral tissue engineering, Acta Biomater. 78 (2018) 365–377, https://doi.org/10.1016/J.ACTBIO.2018.07.039.

[18] G.T. Christopherson, H. Song, H.Q. Mao, The influence of fiber diameter of electrospun substrates on neural stem cell differentiation and proliferation, Biomaterials 30 (2009) 556–564, https://doi.org/10.1016/J.BIOMATERIALS.2008.10.004.

[19] T.L. Jenkins, D. Little, Synthetic scaffolds for musculoskeletal tissue engineering: cellular responses to fiber parameters, NPJ Regen Med 4 (2019) 15, https://doi.org/10.1038/s41536-019-0076-5.

[20] A. Morel, S. Domaschke, V. Urundolil Kumaran, D. Alexeev, A. Sadeghpour, S. N. Ramakrishna, S.J. Ferguson, R.M. Rossi, E. Mazza, A.E. Ehret, G. Fortunato, Correlating diameter, mechanical and structural properties of poly(l-lactide) fibres from needleless electrospinning, Acta Biomater. 81 (2018) 169–183, https://doi.org/10.1016/J.ACTBIO.2018.09.055.

[21] T.L. Jenkins, S. Meehan, B. Pourdeyhimi, D. Little, Meltblown polymer fabrics as candidate scaffolds for rotator cuff tendon tissue engineering, Tissue Eng. 23 (2017), https://doi.org/10.1089/ten.tea.2016.0470.

[22] A.J. Engler, S. Sen, H.L. Sweeney, D.E. Discher, Matrix elasticity directs stem cell lineage specification, Cell 126 (2006) 677–689, https://doi.org/10.1016/J.CELL.2006.06.044.

[23] T. Yeung, P.C. Georges, L.A. Flanagan, B. Marg, M. Ortiz, M. Funaki, N. Zahir, W. Ming, V. Weaver, P.A. Janmey, Effects of Substrate Stiffness on Cell Morphology, Cytoskeletal Structure, and Adhesion, 2004, https://doi.org/10.1002/cm.20041. Cytoskeleton.

[24] R.J. Pelham, Y.L. Wang, Cell locomotion and focal adhesions are regulated by substrate flexibility, Proc. Natl. Acad. Sci. U. S. A. 94 (1997) 13661–13665, https://doi.org/10.1073/PNAS.94.25.13661.

[25] H.J. Nieminen, I. Laidmäe, A. Salmi, T. Rauhala, T. Paulin, J. Heinämäki, E. Hæggström, Ultrasound-enhanced electrospinning, Sci. Rep. 8 (2018) 1–6, https://doi.org/10.1038/s41598-018-22124-z.

[26] Kõrkjas Hakkarainen, Lust Laidmäe, Kogermann Semjonov, Salmi Nieminen, Korhonen, Haeggström, Heinämäki, Comparison of traditional and ultrasound-enhanced electrospinning in fabricating nanofibrous drug delivery systems, Pharmaceutics 11 (2019) 495, https://doi.org/10.3390/pharmaceutics11100495.

[27] M. Herrero-Herrero, S. Alberdi-Torres, M.L. González-Fernández, G. Vilariño-Feltrer, J.C. Rodríguez-Hernández, A. Vallés-Lluch, V. Villar-Suárez, Influence of chemistry and fiber diameter of electrospun PLA, PCL and their blend membranes, intended as cell supports, on their biological behavior, Polym. Test. 103 (2021), 107364, https://doi.org/10.1016/J.POLYMERTESTING.2021.107364.

[28] A.S. Badami, M.R. Kreke, M.S. Thompson, J.S. Riffle, A.S. Goldstein, Effect of fiber diameter on spreading, proliferation, and differentiation of osteoblastic cells on electrospun poly(lactic acid) substrates, Biomaterials 27 (2006) 596–606, https://doi.org/10.1016/J.BIOMATERIALS.2005.05.084.

[29] J. Pelipenko, P. Kocbek, J. Kristl, Critical attributes of nanofibers: preparation, drug loading, and tissue regeneration, Int. J. Pharm. 484 (2015) 57–74, https://doi.org/10.1016/J.IJPHARM.2015.02.043.

[30] N. Bhardwaj, S.C. Kundu, Electrospinning: a fascinating fiber fabrication technique, Biotechnol. Adv. 28 (2010), https://doi.org/10.1016/j.biotechadv.2010.01.004.

[31] I. Sebe, E. Ostorházi, Z. Bodai, Z. Eke, J. Szakács, N.K. Kovács, R. Zelkó, In vitro and in silico characterization of fibrous scaffolds comprising alternate colistin sulfate-loaded and heat-treated polyvinyl alcohol nanofibrous sheets, Int. J. Pharm. 523 (2017) 151–158, https://doi.org/10.1016/J.IJPHARM.2017.03.044.

[32] O.v. Surov, M.I. Voronova, A.v. Afineevskii, A.G. Zakharov, Polyethylene oxide films reinforced by cellulose nanocrystals: microstructure-properties relationship, Carbohydr. Polym. 181 (2018) 489–498, https://doi.org/10.1016/J.CARBPOL.2017.10.075.

[33] D. Kiss, K. Süvegh, T. Marek, L. Dévényi, C. Novák, R. Zelkó, Tracking the physical aging of poly(ethylene oxide): a technical note, AAPS PharmSciTech 7 (2006) E95, https://doi.org/10.1208/pt070495. –E98.

[34] K.W. Ebagninin, A. Benchabane, K. Bekkour, Rheological characterization of poly (ethylene oxide) solutions of different molecular weights, J. Colloid Interface Sci. 336 (2009) 360–367, https://doi.org/10.1016/J.JCIS.2009.03.014.

[35] J.M. Deitzel, J. Kleinmeyer, D. Harris, N.C. Beck Tan, The effect of processing variables on the morphology of electrospun nanofibers and textiles, Polymer 42 (2001) 261–272, https://doi.org/10.1016/S0032-3861(00)00250-0.